Contrib Mineral Petrol (2006) 152:309–321
DOI 10.1007/s00410-006-0103-6

ORIGINAL PAPER

Geochemical constraints on the origin of the Permian Baimazhai mafic–ultramafic intrusion, SW China

Christina Yan Wang · Mei-Fu Zhou · Reid R. Keays

Received: 6 September 2005 / Accepted: 5 April 2006 / Published online: 11 July 2006

Abstract The ~260 Ma Baimazhai mafic–ultramafic intrusion is considered to be part of the Emeishan large igneous province and consists of orthopyroxenite surrounded by websterite and gabbro. The intrusion is variably mineralized with a massive sulfide ore body (~20 vol.%) in the core of the intrusion. Silicate rocks have Ni/Cu ratios ranging from 0.3 to 46 with majority less than 7 and are rich in LREE relative to HREE and show Nb and Ta anomalies in primitive mantle-normalized trace element patterns, with low Nb/Th (1.0–4.5) and Nb/La (0.3–1.0) ratios. Their ε Nd(t) values range from –3.3 to –8.4. Uniform Pd/Pt (0.7–3.5) and Cu/Pd (100,000–400,000) ratios throughout the intrusion indicate that all the sulfides in the rocks were formed in a single sulfide-saturation event. Modeling suggests that the Baimazhai rocks were formed when an Mg-rich magma became crustally contaminated in a deep-seated staging chamber. Crustal contamination (up to ~35%) drove the magma to S-saturation and forced orthopyroxene (Opx) onto the liquidus. The crystal-bearing magma forced out of the staging chamber was migrated by flow differentiation and consequently, the denser sulfide melt and the Opx crystals became centrally disposed in the flowing magma to form the Baimazhai intrusion.

Electronic Supplementary Material Supplementary material is available to authorised users in the online version of this article at http://dx.doi.org/10.1007/s00410-006-0103-6.

Communicated by T. L. Grove

C. Y. Wang (✉) · M.-F. Zhou
Department of Earth Sciences, University of Hong Kong, Hong Kong, China
e-mail: wangyan2002@hkusua.hku.hk

R. R. Keays
Mineral Exploration Research Centre, Laurentian University, Sudbury, ONT, Canada

R. R. Keays
VIEPS, School of Geosciences, Monash University, Melbourne, VIC, Australia

Introduction

Crustal contamination is an important process that modifies geochemically mantle-derived magmas. Such a process is often associated with fractional crystallization (AFC) and explains geochemical differences between continental flood basalts and ocean island basalts or enriched mid-ocean-ridge basalts (Mahoney 1988; Arndt et al. 1993). It has also been widely documented that crustal contamination was a very likely trigger to S-saturation in mafic magmas to form Ni–Cu–(PGE) sulfide deposits (Brugmann et al. 1993; Naldrett 2004; Lightfoot and Keays 2005). However, it is still unclear what the contaminants were and at what stage in the evolution of the magmas the contamination took place.

The Permian (~260 Ma) Emeishan large igneous province (ELIP) consists of the Emeishan continental flood basalts and mafic–ultramafic intrusions in SW China and northern Vietnam. The intrusions are hosts of giant oxide ore deposits, such as the Panzhihua intrusion (Zhou et al. 2005), and Ni–Cu–(PGE) sulfide deposits, such as the Yangliuping intrusion (Song et al. 2003) and Jinbaoshan intrusion (Wang et al. 2005a).

The diversity of ELIP rocks was explained by different mantle sources or mantle plume-lithosphere interaction (Chung and Jahn 1995; Song et al. 2001; Xu et al. 2001). The role of crustal contamination in the generation of ELIP rocks and associated sulfide ore deposits are not well understood. In the southern part of the ELIP, the Baimazhai mafic–ultramafic intrusion is spatially associated with the Emeishan flood basalts and contains Ni–Cu–(PGE) sulfide mineralization. The intrusion is a concentric body with an inner core of orthopyroxenite surrounded by websterite, which in turn, is rimmed by gabbro. It is possible that the intrusion formed from Si- and Mg-rich mafic magmas, similar to siliceous high-Mg basalts (SHMB) that were explained by heavily crustal contamination from komatiites (Sun et al. 1989). Thus it provides an opportunity to evaluate the role of crustal contamination in the generation of the Baimazhai intrusion and its ore formation.

In this contribution, we report new SHRIMP zircon U–Pb isotopic analyses that yield an age of ~260 Ma for the Baimazhai intrusion, an age that is consistent with the age of the ELIP (Zhou et al. 2002a, 2005, 2006). We present the results of a systematic geochemical study of samples collected from diamond drill holes that penetrated the entire intrusion. We also carried out PGE analyses for a complete set of drill core samples, which are compared to similar intrusions elsewhere. Our major goals are to better understand the genetic relationships between the different rock units within the Baimazhai intrusion, to examine the role of crustal contamination in the formation of the intrusion and its sulfides and to investigate possible contaminants and relative timing of contamination. We also discuss factors responsible for the concentric form of the intrusion.

Geological background

The ELIP is exposed over a large part of SW China and northern Vietnam from the eastern margin of the Tibetan Plateau to the western margin of the Yangtze Block (Fig. 1a). The Emeishan volcanic succession comprises predominantly basaltic flows and pyroclastics with minor amount of picrite and basaltic andesite, and covers an area of more than 5×10^5 km^2 with thickness ranging from several hundred meters up to 5 km (Chung and Jahn 1995; Song et al. 2001; Xu et al. 2001) (Fig. 1a). The western part of the ELIP was affected by the Cenozoic collision of the Indian and Eurasian Plates. In the Panzhihua–Xichang region, the central part of the ELIP, numerous mafic–ultramafic intrusions are exposed because of uplift along numerous N–S-trending faults and are hosts of major oxide deposits (Zhou et al. 2005). In the southernmost part of the Yangtze Block, many mafic–ultramafic dykes and layered intrusions within Ordovician and Devonian strata are spatially associated with the Permian flood basalts. These intrusive bodies occur across the border between China and Vietnam, forming a belt running in a NW–SE direction, SW of the Ailao Shan-Red River (ASRR) strike-slip fault zone (Fig. 1a).

In the Jinping region, the ASRR fault zone has uplifted metamorphic rocks. South of the fault zone, Ordovician, Devonian, Carboniferous, Permian and Triassic strata are well developed, whereas north of the fault zone, a large area is covered by Triassic strata. The Ordovician strata are composed of interlayered meta-slates and meta-sandstone, whereas the Devonian and Carboniferous strata consist of limestones with interlayered shales and cherts. The Permian Emeishan basaltic succession has a thickness of up to 4.5 km and unconformably overlies limestones of the early Permian Maokou Formation (YBGMR 1990). The basaltic association consists of volcanic breccia, massive aphyric basalt, plagioclase (Pl)-dominated phaneritic basalt, amygdaloidal basalt and minor amount of interbedded tuff. The Triassic strata consist of neritic sedimentary carbonates with coal measures.

In Jinping, undifferentiated mafic dykes/sills occur along the sedimentary bedding of the Devonian strata. In the Baimazhai area northwest of Jinping, a group of small, differentiated intrusions including the Baimazhai intrusion intrude the Ordovician meta-sandstones and slates (Fig. 1a, b) but only the Baimazhai intrusion hosts Ni–Cu–(PGE) sulfide ore deposit.

Petrography of the Baimazhai intrusion

The Baimazhai intrusion has a surface exposure of 0.1 km^2 (Fig. 1b). The intrusion trends 296° and dips 22°N and is 530 m in length, 190 m in width and 24–64 m in thickness, as demonstrated by an extensive drill and exploration program conducted by local geological teams. The intrusion itself was intruded by lamprophyre dykes that are possibly Cenozoic in age (Guan et al. 2003).

The intrusion has a lens-like shape in the cross section (Fig. 1c). Major rock types include orthopyroxenite, websterite and gabbro, which form a concentric body with an inner core of orthopyroxenite surrounded by websterite, which in turn, is rimmed by gabbro. The orthopyroxenite exhibits a poikilitic texture consisting of ~90 vol.% orthopyroxene (Opx)

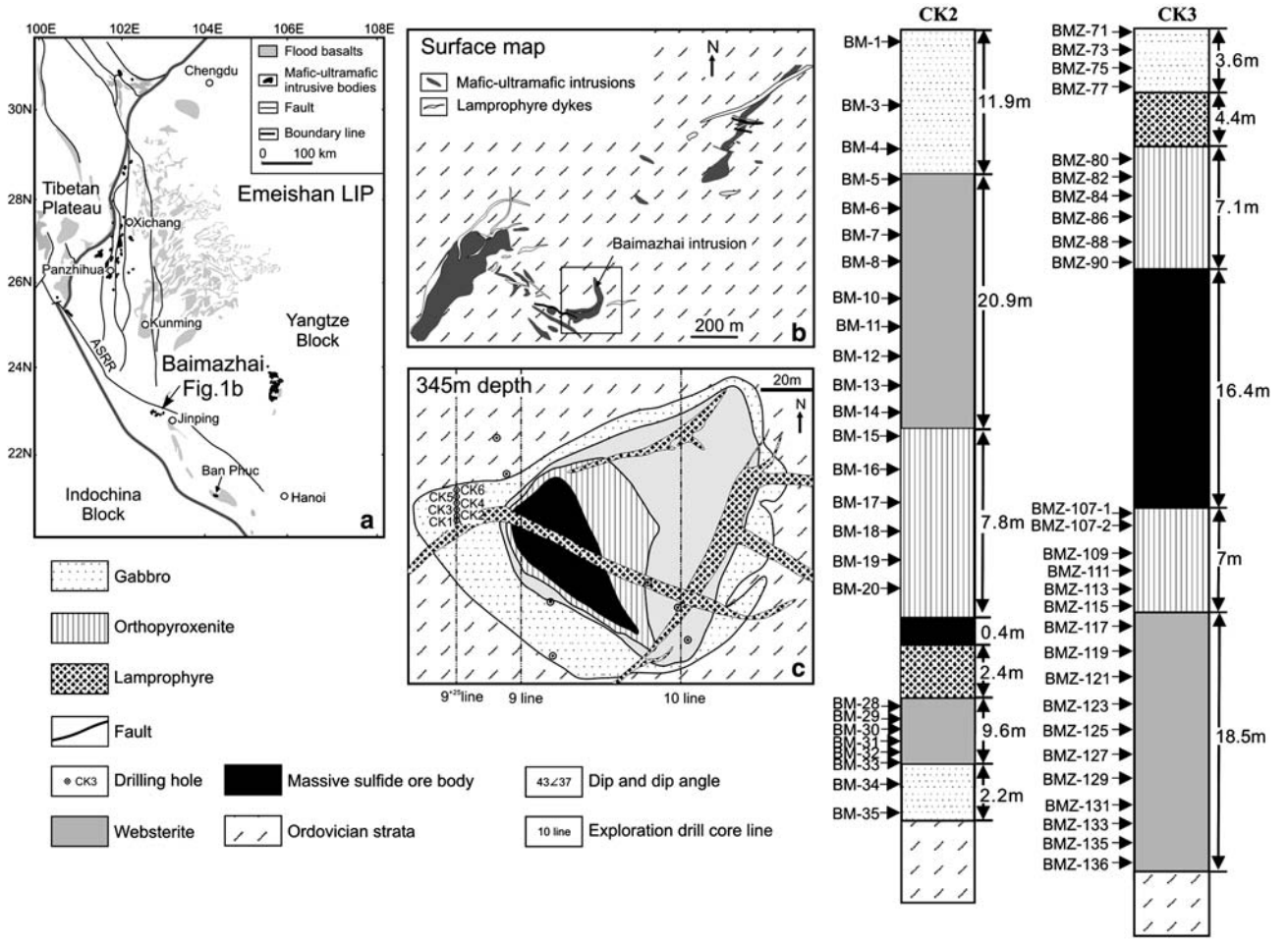

Fig. 1 **a** Simplified geological map showing the occurrence of the Emeishan large igneous province in SW China and Northern Vietnam and the tectonic location of the Baimazhai intrusion (modified from Zhou et al. 2002a and Geological map of Vietnam); **b** a surface map showing the mafic–ultramafic intrusions in the Baimazhai area (after Jinping Nickel Mine, 2002) and **c** a planar of the Baimazhai intrusion at 345 m depth, showing the distribution of rock units (after the Jinping Nickel Mine, 2002). Relative positions of each sample are shown in the *columns* of drill cores CK2 and CK3

phenocrysts and ~10 vol.% interstitial clinopyroxene (Cpx). Extensive alteration of the rocks resulted in replacement of the bulk of the Opx by cummingtonite and the Cpx by tremolite, although relict hypersthene can be still observed in some phenocrysts. The websterite is also strongly altered with Cpx, Opx and Pl replaced by tremolite, cummingtonite and albite, respectively. It was probably composed of Opx (~50 vol.%), Cpx (~45 vol.%) and minor Pl (~5 vol.%). The gabbro now consists of tremolite and albite with minor amounts of biotite, quartz, ilmenite and apatite. Textural and paragenetic relationships demonstrate that the order of crystallization of the silicates was Opx $\rightarrow$ Opx + Cpx $\rightarrow$ Cpx + Pl. Subsequently, the intrusion underwent low grade amphibolite facies metamorphism.

Two drill cores which provided the samples for this study penetrated a massive sulfide ore body in the core of the intrusion (0.4 to ~16 m in thickness). The proportion of gabbro, websterite, orthopyroxenite and massive sulfide ore body is approximately 30, 30, 20 and 20 vol.%, respectively. The gabbros contain <1 wt% sulfide, whereas the websterites are mineralized with disseminated sulfides varying from 0.11 to 17 wt%. The inner core orthopyroxenites are almost totally mineralized with net-textured sulfides ranging from 1.2 to 61 wt%. The massive ores contain sulfides varying from 52 to 88 wt%. The massive and net-textured ores have similar ore minerals and consist of pyrrhotite (~40–74 vol.%), pentlandite (3–12 vol.%), chalcopyrite (1–19 vol.%) and magnetite (2–8 vol.%).

Analytical methods

Major element oxides

For S-poor samples (S<1 wt%), major element oxides were determined by wavelength-dispersive X-ray fluorescence spectrometry (WD-XRFS) on fused glass beads using a Philips PW2400 spectrometer at the University of Hong Kong. The accuracies of the XRF analyses are estimated to be ±2% (relative) for major oxides present in concentrations greater than 0.5 wt% and ±5% (relative) for minor oxides greater than 0.1 wt%. Sulfur abundances were obtained by the Leco method at the Geoscience Laboratories, Sudbury, Canada.

For S-rich samples, major element oxides (except SiO_2) were obtained using inductively coupled plasma atomic emission spectroscopy (ICP-AES) at the Guangzhou Institute of Geochemistry, Chinese Academy of Sciences (CAS). The precision of the analyses were generally better than 1% when element concentration greater than 200 ppm, and 1–3% when less than 200 ppm. Silica and S were obtained separately using a gravimetric method at the University of Hong Kong.

Trace elements

Selected trace elements, including V, Cr, Ni and Cu, were analyzed by WD-XRFS of pressed powder pellets for S-poor samples at the University of Hong Kong, and by ICP-AES of solutions for S-rich samples at the Guangzhou Institute of Geochemistry. Additional trace elements were determined by inductively coupled plasma mass spectrometry (ICP-MS) using a VG Plasma-Quad Excell ICP-MS at the University of Hong Kong after a 2-day closed-beaker digestion using a mixture of HF and HNO_3 acids in high-pressure bombs (Qi et al. 2000). The accuracies of the ICP-MS analyses are estimated to be better than ±5% (relative) for most elements.

PGE analyses

The PGE analyses were performed using the ICP-MS at the University of Hong Kong after NiS fire assay and Te-precipitation for sulfide-rich samples, and a Carius tube dissolution for sulfide-poor samples. For the NiS fire assay method (Zhou et al. 2001), the standard reference materials used in the procedure were WMS-1 (a sulfide ore) and WPR-1 (an ultramafic rock). The accuracy is estimated to be better than 5% for Rh, Pd and Ir, and 10% for Pt. The procedural blanks for the technique were 0.23 ppb Ru, 5.79 ppb Pd, 0.10 ppb Ir, 0.81 ppb Pt and 0.06 ppb Rh. For the Carius tube method (L. Qi et al., submitted for publication), the total procedural blank was less than 0.003 ppb for Ru, Rh and Ir, 0.020 ppb for Pd, and 0.011 ppb for Pt. The accuracy is estimated to be better than 5% for Rh, Pd and Ir, and Pt.

Rb–Sr and Sm–Nd isotopic analyses

Isotope ratios of Sr–Nd and concentrations of Rb, Sr, Sm and Nd were determined on a VG-354 thermal ionization magnetic sector mass spectrometer at the Institute of Geology and Geophysics, CAS, Beijing. The chemical separation and isotopic measurement procedures are described in Zhang et al. (2001). Mass fractionation corrections for Sr and Nd isotopic ratios were based on values of $^{86}Sr/^{88}Sr=0.1194$ and $^{146}Nd/^{144}Nd=0.7219$. Uncertainties in Rb/Sr and Sm/Nd ratios are less than ±2 and ±0.5% (relative), respectively.

Analytical results

SHRIMP zircon analytical results

The detailed analytical method is described in Wang et al. (2005b). A gabbro sample (BM34) contains numerous zircon grains with a variety of morphologies indicating a magmatic origin. The SHRIMP analytical results (15 spots on 15 grains) for this sample are listed in Table 1. Nine analyses have moderate Th/U ratios (1.45–2.90) and yield an average $^{206}Pb/^{238}U$ age of 258.5±3.5 Ma, which can be considered as the crystallization age of the gabbro (Fig. 2).

Five zircon grains have ages older than 400 Ma (Table 1). All these grains have Th/U ratios between 0.34 and 0.64, much lower than those for 258.5 Ma zircon grains. These older zircons are interpreted to be xenolithic in origin.

Major element oxides

Representative major oxides of the Baimazhai intrusion are listed in Table S1. In order to interpret the lithophile element chemistry of the Baimazhai samples, it was necessary to recast the whole rock raw data on a sulfide-free basis (the procedure is not shown in this paper, but available on request from the senior author). Although the recast anhydrous oxide values are inaccurate, there are such large variations from sample to sample that it is still possible to follow trends.

Table 1 U–Pb SHRIMP analytical results of zircons from a gabbro (BM34) of the Baimazhai intrusion, Jinping, SW China

Spot	$^{206}Pb_c$ (%)	Concentration (ppm)			Th/U	Calculated ratios						Calculated ages (Ma)			
		U	Th	$^{206}Pb^*$		$^{206}Pb^*/^{238}U$	±%	$^{207}Pb^*/^{235}U$	±%	$^{207}Pb^*/^{206}Pb^*$	±%	$^{206}Pb/^{238}U$		$^{207}Pb/^{206}Pb$	
BM34-1	0.00	306	155	33.0	0.52	0.12550	2.1	1.109	2.4	0.0640	1.0	762	±15	743	±21
BM34-2	0.06	2,345	5,887	84.2	2.59	0.04178	2.1	0.300	2.2	0.0521	0.72	264	±5.4	289	±16
BM34-3	0.38	1,444	3,163	50.7	2.26	0.04067	2.1	0.278	3.1	0.0496	2.3	257	±5.4	176	±53
BM34-4	0.12	5,628	13,430	199	2.47	0.04111	2.1	0.282	2.6	0.0497	1.5	260	±5.4	181	±36
BM34-5	0.62	498	307	48.2	0.64	0.11200	2.3	0.948	3.3	0.0614	2.4	685	±15	653	±51
BM34-6	0.18	3,117	6,955	108	2.31	0.04021	2.1	0.284	2.5	0.0512	1.4	254	±5.3	249	±31
BM34-7	0.17	2,665	6,208	91.5	2.41	0.03988	2.1	0.275	2.5	0.0500	1.2	252	±5.2	196	±29
BM34-8	0.21	238	77	59.3	0.34	0.28990	2.2	4.650	2.4	0.1162	0.98	1,641	±32	1,899	±18
BM34-9	0.08	4,334	10,008	152	2.39	0.04073	2.1	0.285	2.3	0.0508	0.92	257	±5.3	231	±21
BM34-10	0.44	940	1,383	30.6	1.52	0.03775	2.2	0.257	3.7	0.0494	2.9	239	±5.1	165	±69
BM34-11	0.09	3,492	9,784	118	2.90	0.03946	2.1	0.271	2.4	0.0498	1.1	250	±5.2	187	±25
BM34-12	0.18	203	113	21.6	0.58	0.12360	2.1	1.049	2.6	0.0615	1.5	752	±15	658	±33
BM34-13	0.05	1,591	3,057	57.1	1.99	0.04177	2.1	0.292	2.3	0.0507	1.0	264	±5.4	228	±24
BM34-14	0.15	1,255	2,019	46.4	1.66	0.04299	2.1	0.296	2.4	0.0499	1.1	271	±5.6	190	±26
BM34-15	0.00	100	62	5.49	0.64	0.06400	2.3	0.497	3.3	0.0563	2.4	400	±8.8	464	±54

Errors are 1-sigma; Pb_c and Pb* indicate the common and radiogenic portions, respectively. Error in standard calibration was 0.48% (not included in above errors but required when comparing data from different mounts). Common Pb corrected using measured ^{204}Pb

The websterites and orthopyroxenites have much lower SiO_2 and Al_2O_3 but higher FeO_{total} and MgO than the gabbros. The mineralogical phases which control the composition of the rocks can be determined using the Pearce element ratio plot of the molar ratio (Mg + Fe)/Si against the molar ratio Si/Ti, all of the websterite and orthopyroxenite samples fall roughly on the Opx control line (Fig. 3). In particular, none of the Baimazhai samples plot close to the olivine control line. It is clear that the orthopyroxenites were mostly controlled by Opx accumulation. Cpx and Opx were major fractionating phases in the websterites; and Pl was a major fractionating phase in the gabbros. The Pearce element ratio plot hence supports the observed mineral assemblages.

Trace elements

In general, all silicate rocks have similar chondrite-normalized REE patterns with LREE enrichment (Fig. 4a–c). The gabbros have relatively high REE contents compared to the websterites and orthopyroxenites. The gabbros have either weakly negative or positive Eu anomalies, whereas the websterites and orthopyroxenites have relatively large negative or positive Eu anomalies.

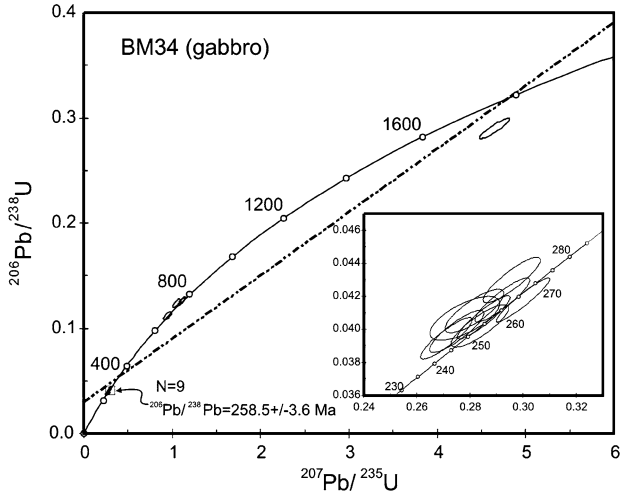

Fig. 2 SHRIMP zircon U–Pb concordia plot for gabbro BM34 from the Baimazhai intrusion (see Fig. 1 for sample location)

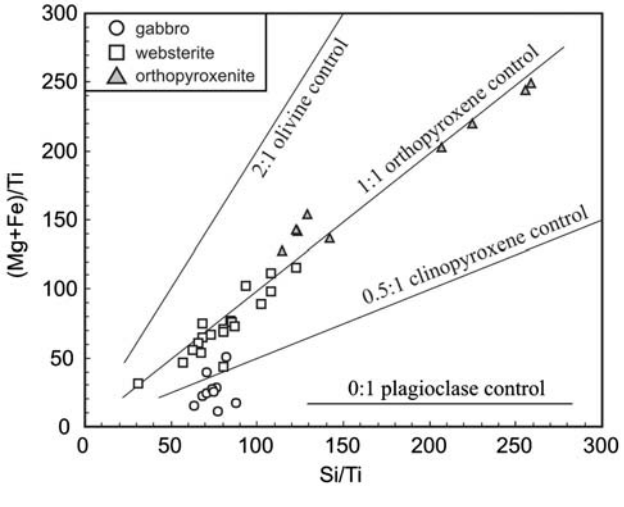

Fig. 3 Pearce element ratios diagram showing the dominant phase is *Opx*

On primitive mantle-normalized trace element spidergrams (Fig. 5), Rb, Ba and Sr have larger variations than other elements, probably due to their mobile nature during alteration. Thorium exhibits positive anomalies, whereas Sr displays either negative or positive anomalies. All samples have slightly negative Nb and Ta anomalies. The gabbros also have negative Ti anomalies (Fig. 5a). The orthopyroxenites and websterites have both negative and positive Ti anomalies (Fig. 5b, c); the positive Ti anomalies may correspond to high sulfide contents and therefore, high magnetite contents associated with sulfides.

Cu, Ni and PGEs

The PGE data from one set of drill core samples are listed in Table 2. All the rocks have variable Pd/Ir ratios ranging from 4 to 183. Throughout the intrusion Pd/Pt ratios vary from 0.78 to 3.50 and Cu/Pd ratios from 30,000 to 1,500,000 (most from 100,000 to 400,000). Both sulfide-poor gabbros and sulfide-rich orthopyroxenites and websterites have similar chondrite-normalized chalcophile element patterns

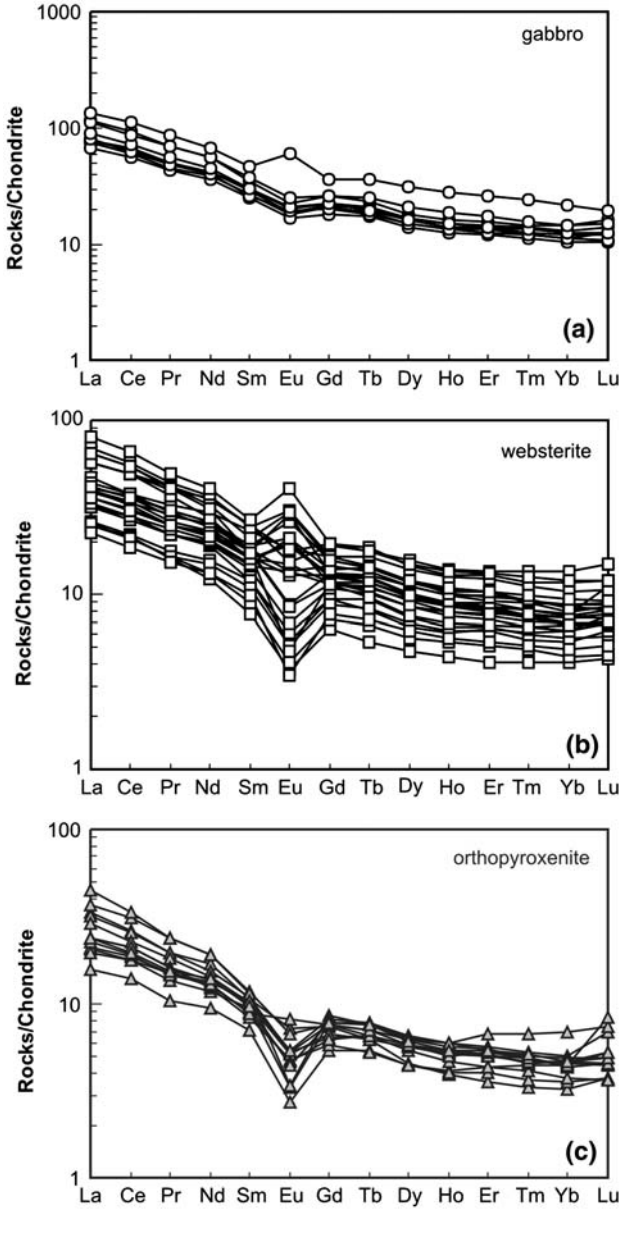

Fig. 4 Chondrite-normalized REE patterns of the rocks from the Baimazhai intrusion. Normalization values are from Sun and McDonough (1989)

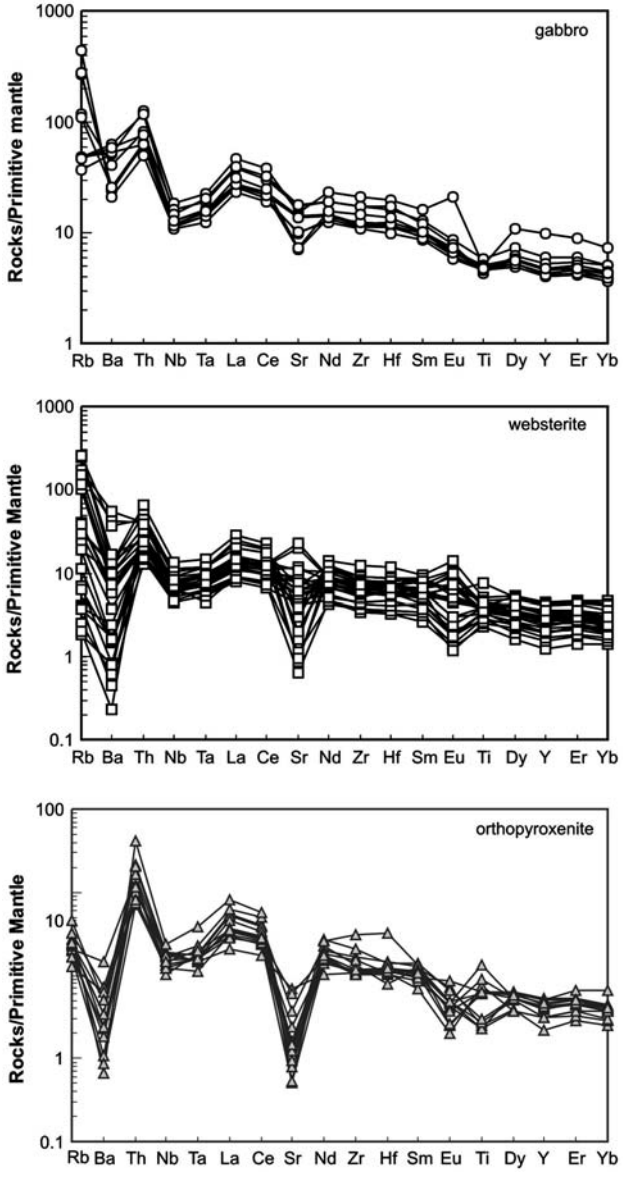

Fig. 5 Primitive mantle-normalized trace element patterns of the Baimazhai intrusion. Normalization values are from Sun and McDonough (1989)

(Fig. 6a–c). The similarity in the patterns together with similar Pd/Pt, Cu/Pd and, to a lesser extent, Pd/Ir ratios suggests that the sulfides of the various rock types are co-genetic.

The Cu and Ni contents of the Baimazhai intrusion vary as a function of their S and sulfide contents. The orthopyroxenites contain 1.2–60.9 wt% sulfides and have variable but generally higher Cu and Ni contents than the websterites. The gabbros have very low sulfide contents and therefore low Ni and Cu contents (from 0.002 to 0.03 wt% and from 0.002 to 0.02 wt%, respectively). All silicates have Ni/Cu ratios less than 7 with a range from 0.5 to 6.7.

The Cu/Zr ratios of the silicate rocks of the Baimazhai intrusion vary widely, from 0.08 to 2,240 and correlate positively with sulfide content (Fig. 7a). On a Pt/Y versus Pd/Cr scattergram, the Pt/Y ratios vary positively with the Pd/Cr ratios (Fig. 7b).

Rb–Sr and Sm–Nd isotopic compositions

Sm–Nd isotopic compositions of the Baimazhai rocks are relatively constant with $^{143}Nd/^{144}Nd$ ratios ranging from 0.51212 to 0.51239 and $\varepsilon Nd(t)$ values ranging from –3.3 to –8.4, whereas the initial $^{87}Sr/^{86}Sr$ ratios vary widely from 0.7032 to 0.7188 (Table 3). There is a positive relationship between $\varepsilon Nd(t)$ values and Nb/La ratios (Fig. 8). The $\varepsilon Nd(t)$ values of the gabbros are lower than those of the websterites and orthopyroxenites. The $\varepsilon Nd(t)$ values and Nb/La ratios of the gabbros and orthopyroxenites are lower than the range of the Emeishan continental flood basalts.

Discussion

Alteration effects

The Baimazhai intrusion has undergone strong alteration during low amphibolite facies metamorphism. Previous studies have suggested that under such metamorphic conditions, Al, Ca and Mg are relatively immobile (e.g., Beswick 1982).

The intrusion is cut by numerous lamprophyre dykes and minor diabase dykes. The intrusion of the lamprophyric magmas may have locally introduced K, Rb,

Table 2 PGE contents of the rocks from the Baimazhai intrusion, Jinping, SW China

Sample No.	S (wt%)	Sulfide (wt%)	Ni (ppm)	Cu (ppm)	Ir (ppb)	Ru (ppb)	Rh (ppb)	Pt (ppb)	Pd (ppb)
Orthopyroxenites									
BMZ-80	2.84	7.57	3,084	4,920	0.14	0.20	0.10	4.15	3.23
BMZ-82	17.98	47.0	17,592	4,611	2.65	1.90	1.04	47.1	54.3
BMZ-84	10.60	27.7	10,496	1,572	1.34	0.94	0.43	22.3	44.3
BMZ-86	11.06	29.2	10,644	13,178	0.83	0.50	0.28	14.0	22.0
BMZ-88	15.34	40.6	13,196	24,411	0.95	0.56	0.35	28.5	46.6
BMZ-90	20.40	53.4	23,039	5,746	1.4	0.78	0.56	45.9	86.8
BMZ-107-1	22.94	60.4	26,802	13,927	3.87	5.13	0.88	23.1	30.4
BMZ-107-2	18.77	49.3	21,142	11,079	4.03	5.92	0.77	13.0	17.5
BMZ-109	0.49	1.19	1,578	251	0.08	0.14	0.06	1.20	1.76
BMZ-111	6.03	15.9	6,586	5,250	0.32	0.40	0.35	14.6	17.4
BMZ-113	5.61	14.9	5,884	8,841	0.44	0.48	0.21	44.6	80.2
BMZ-115	0.62	1.65	1,075	539	0.06	0.13	0.06	1.52	2.60
Websterites									
BMZ-117	0.45	1.20	840	508	0.07	0.20	0.06	0.74	1.94
BMZ-119	0.23	0.61	449	119	0.04	0.10	0.02	0.23	0.69
BMZ-121	1.94	5.05	1,399	710	0.31	0.46	0.14	2.90	8.90
BMZ-123	1.02	2.67	901	412	0.14	0.26	0.08	0.98	1.72
BMZ-125	0.89	2.34	1,087	467	0.07	0.15	0.06	1.11	1.61
BMZ-127	0.97	2.55	1,084	460	0.07	0.16	0.06	0.76	1.83
BMZ-129	2.04	5.44	3,522	1,937	0.22	0.53	0.19	2.65	5.32
BMZ-131	1.19	3.14	1,561	752	0.09	0.19	0.08	1.02	2.35
BMZ-133	1.43	3.72	1,052	435	0.07	0.16	0.06	0.78	2.34
BMZ-135	0.39	1.03	538	169	0.05	0.15	0.03	0.97	1.56
BMZ-136	0.06	0.16	289	62.8	0.03	0.17	0.01	0.31	0.59
Gabbros									
BMZ-71	0.04	0.12	49.8	21.2	0.02	0.05	0.01	0.08	0.19
BMZ-73	0.16	0.42	118	46.4	0.07	0.33	0.05	0.41	0.43
BMZ-75	0.16	0.42	139	57.7	0.02	0.06	0.01	0.18	0.63
BMZ-77	0.23	0.61	281	133	0.03	0.07	0.02	0.24	0.60

BMZ71–80 and 111–136 were measured by Carius Tube method, BMZ82–109 are measured by fire assay method

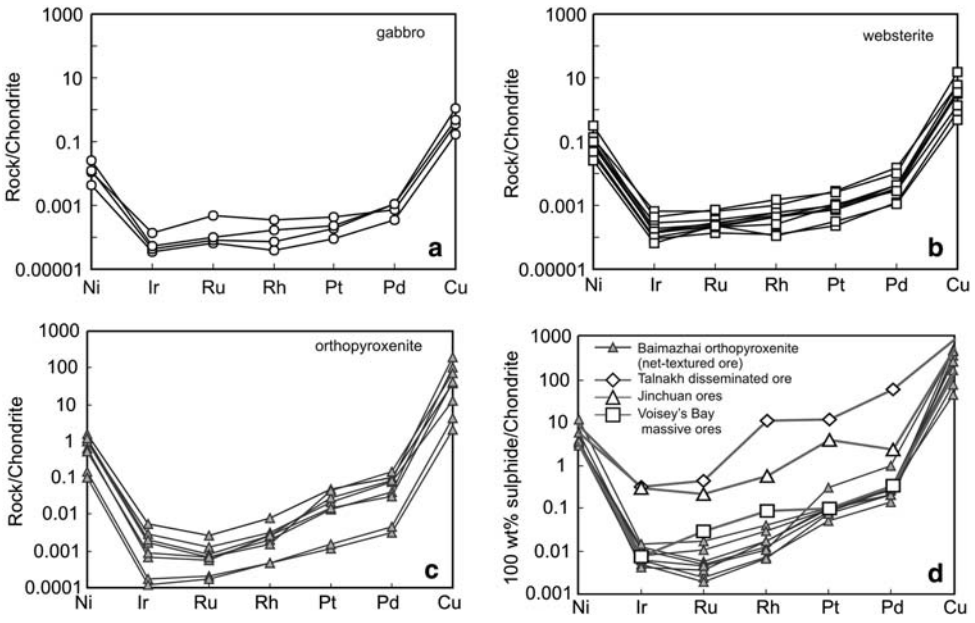

Fig. 6 Chondrite-normalized chalcophile element patterns of the rocks from the Baimazhai intrusion (**a**, **b**, **c**) and comparison of the Baimazhai orthopyroxenites (net-textured ores) with ores of some other deposits related to mafic intrusions (**d**). Normalization values are from Anders and Grevesse (1989). Ore compositions are recalculated to 100% sulfide. Data sources: Voisey's Bay and Talnakh from Naldrett (2004) and Jinchuan from Chai and Naldrett (1992)

Sr and Ba. Large variation of $^{87}Sr/^{86}Sr$ ratios may also likely reflect the alteration effects. However, high field strength elements (HFSE), such as Th, Zr, Hf, Nb, Ta, Ti, Y and REE including Sm–Nd isotopic system, and PGEs, may have remained immobile (Barnes et al. 1985). Therefore, we believe that the εNd(t) values and the reported values of HFSE in this study reflect those of the original magmatic rocks.

Genesis of the Baimazhai intrusion by the Emeishan mantle plume

Eruption of the Emeishan continental flood basalts is considered to coincide with the end-Guadalupian mass extinction dated at ~260 Ma for the mafic intrusions that are spatially associated with the flood basalts (Zhou et al. 2002a). Previous studies favor a mantle plume-related origin for the ELIP (Chung and Jahn 1995; Song et al. 2001; Xu et al. 2001; Zhou et al. 2006). The Baimazhai intrusion is dated at ~259 Ma using SHRIMP zircon U–Pb technique (Fig. 2) and is spatially associated with the Emeishan flood basalts in Jinping (Fig. 1a), supporting the view that it is also part of the ELIP and was produced by the same mantle plume at ~260 Ma.

The composition of magmas parental to the Baimazhia intrusion is difficult to estimate as it does not have obvious chilled margins that can be used to estimate parental magma compositions, and olivine was not the dominant mineral phase, and the rocks were heavily contaminated by crustal materials (see next section). However, ratios of chalcophile elements (Ni, Cu and PGE) may remain constant during crustal contamination and can be used for discussing the parental magma composition (Keays 1995). Ultramafic magmas usually give rise to Ni-dominated sulfide deposits with Ni/Cu ratios higher than 7, such as the volcanic peridotite associated Ni deposits of Kambalda, Western Australia (Ni/Cu = 13.5) (Lesher et al. 1984). Mafic magmas commonly produce Ni–Cu–(PGE) sulfide deposits with Ni/Cu usually less than 2 (Naldrett 2004). Examples of these include those of

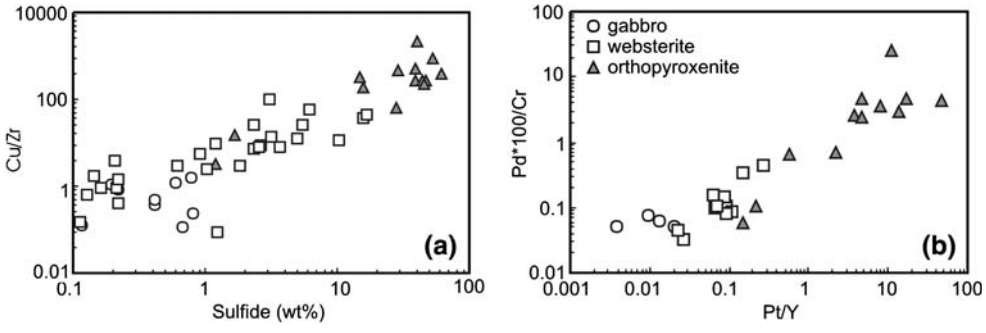

Fig. 7 Cu/Zr versus sulfide (**a**) and Pt*/Y versus Pd*100/Cr (**b**) for the rocks of the Baimazhai intrusion

Table 3 Sm–Nd and Rb–Sr isotopic analytical results of the rocks from the Baimazhai intrusion, Jinping, SW China

Samples	Rb (ppm)	Sr (ppm)	$^{87}Rb/^{86}Sr$	$^{87}Sr/^{86}Sr$	2σ	$(^{87}Sr/^{86}Sr)i$	Sm (ppm)	Nd (ppm)	$^{147}Sm/^{144}Nd$	$^{143}Nd/^{144}Nd$	2σ	$(^{143}Nd/^{144}Nd)_i$	$\varepsilon Nd(t)$
Baimazhai intrusion													
BM-3	36.10	146.07	0.715	0.718471	0.000020	0.7158	3.97	17.37	0.1382	0.512208	0.000012	0.51197	–6.5
BM-5	4.80	61.14	0.226	0.717139	0.000014	0.7163	3.75	15.15	0.1497	0.512130	0.000012	0.51188	–8.4
BM-7	6.70	12.33	1.581	0.715614	0.000017	0.7098	1.30	5.47	0.1436	0.512377	0.000013	0.51213	–3.3
BM-9	3.20	6.43	1.441	0.717557	0.000015	0.7122	1.50	6.33	0.1436	0.512373	0.000010	0.51213	–3.4
BM-13	19.40	17.37	3.233	0.720265	0.000017	0.7084	3.05	13.34	0.1382	0.512192	0.000009	0.51196	–6.8
BM-16	3.90	7.12	1.603	0.714001	0.000020	0.7081	0.79	3.40	0.1401	0.512240	0.000014	0.51200	–5.9
BM-20	1.57	7.01	0.651	0.717276	0.000020	0.7149	0.44	1.74	0.1539	0.512267	0.000016	0.51201	–5.8
BM-24	79.30	39.59	5.806	0.722401	0.000025	0.7010	0.99	4.14	0.1445	0.512255	0.000015	0.51201	–5.8
BM-26	66.60	39.23	4.917	0.721326	0.000014	0.7032	0.79	3.25	0.1470	0.512231	0.000014	0.51198	–6.3
BM-29	14.50	147.80	0.283	0.719795	0.000020	0.7188	2.60	10.36	0.1518	0.512346	0.000007	0.51209	–4.2
BM-32	141.10	211.27	1.936	0.725595	0.000025	0.7185	3.23	11.89	0.1641	0.512389	0.000015	0.51211	–3.8
BM-35	22.90	306.64	0.216	0.722103	0.000020	0.7213	7.18	29.66	0.1463	0.512121	0.000014	0.51187	–8.4
Country rocks (Ordovician sandstone)													
BMZ-146	129.9	78.97	4.779	0.739817	0.000011	0.7099	10.87	48.36	0.1361	0.511846	0.000012	0.5115	–12.1
BMZ-201	129.6	82.41	4.529	0.734357	0.000010	0.7060	9.23	43.79	0.1276	0.511808	0.000009	0.5114	–12.3
BMZ-209	151.4	225.1	1.939	0.723098	0.000010	0.7109	9.51	44.61	0.1291	0.511774	0.000013	0.5114	–13.1
Emeishan picrite (primary magma composition)													
HK–41[a]	2.25	102	0.0636	0.704362	0.000014	0.7041	2.07	4.40	0.2854	0.513146	0.000013	0.5127	+7.0
SM–15[b]	7.33	169	0.1256	0.702648		0.7042	4.18	18.37	0.1375	0.512682		0.5125	+2.7

λ (^{87}Rb)=1.42 × 10^{-11} $year^{-1}$, λ (^{147}Sm)=6.54 × 10^{-12} $year^{-1}$. εNd values were calculated relative to present-day chondrite values of $^{143}Nd/^{144}Nd$=0.512638, $^{147}Sm/^{144}Nd$=0.1967, $^{87}Sr/^{86}Sr$=0.7045 and $^{87}Rb/^{86}Sr$=0.0827. Initial ratios were calculated assuming age of 260 Ma for Baimazhai samples and 440 Ma for the country rocks

[a]Data source from our unpublished data

[b]Data source after Zhang et al. 2004

Noril'sk, Russia (Ni/Cu = 0.5–1.06) and Voisey's Bay, Canada (Ni/Cu = 1.87). As shown in Table 2, the Baimazhai samples have average Ni/Cu ratios of 2.6 with a small range from 0.5 to 6.7. Therefore, the Baimazhai intrusion may not have derived from an ultramafic magma.

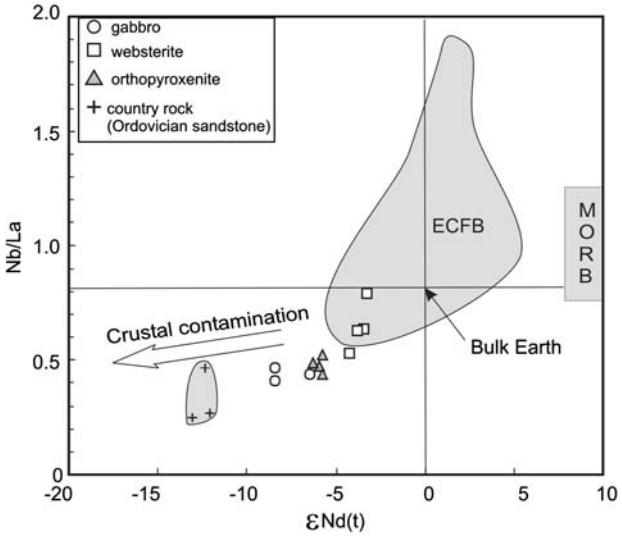

Fig. 8 εNd(*t*) versus Nb/La diagram of the rocks of the Baimazhai intrusion. Emeishan continental flood basalt (*ECFB*) area is after Xu et al. (2001)

PGE data for the Baimazhai orthopyroxenites are compared with those for other bodies on chondrite-normalized chalcophile element plot (Fig. 6d). The Baimazhai orthopyroxenites have relatively steep patterns, similar to the patterns exhibited by the Voisey's Bay, Talnakh and Jinchuan deposits that are associated with igneous bodies formed from magnesian basaltic magmas, but different from those of komatiite-related sulfide ores that usually have relatively flat PGE profiles (Naldrett and Duke 1980). Therefore, the parental magma of the Baimazhai intrusion is also assumed to be Mg-rich, perhaps picritic.

Crustal contamination

The Baimazhai intrusion contains abundant Opx, suggesting the magma from which the Opx crystallized is also Si-rich. Such Si- and Mg-rich magmas would have formed from mantle-derived magmas by heavily crustal contamination from a high-Mg magma as invoked for SHMB (Sun et al. 1989). Abundant xenolithic zircon grains identified (Table 1) are supportive of such crustal contamination. Other evidence for such heavy

crustal contamination includes the negative Nb (Ta) and Ti anomalies of the gabbros and the large negative εNd(t) values (–3.3 to –8.4) of the rocks (Table 3).

The extent of crustal contamination of the magmas which formed the Baimazhai rocks can be estimated using $(Nb/Th)_{PM}$ and $(Th/Yb)_{PM}$ ratios where the rock values have been normalized to the relevant trace element content of the primitive mantle. $(Nb/Th)_{PM}$ is best used to indicate the extent of Nb anomaly whereas $(Th/Yb)_{PM}$ is a sensitive indicator of crustal contamination. Compared to N-MORB, the Baimazhai rocks have very low $(Nb/Th)_{PM}$ but high $(Th/Yb)_{PM}$ ratios, consistent with a high degree of crustal contamination (Fig. 9). The degree of crustal contamination can be estimated by assuming that the rock compositions observed are products of the mixing of a mantle-derived magma and a crustal contaminant. For the mantle-derived end member, we used two compositions, one being N-MORB (Sun and McDonough 1989) and the other the average of two analyses of the most primitive and least contaminated low Ti, high Mg picrites of the ELIP (Table S1). For the crustal end member, we used the average composition of the Ordovician sandstones which are the country rocks of the Baimazhai intrusion, representing the upper crustal rocks of the Yangtze Block. Using the average composition of the Emeishan picrites as the mantle-derived end member gives a good fit to the Baimazhai data, whereas the use of N-MORB as an end member gives a poorer fit (Fig. 9). The average composition of the Kangding basement complex of the Yangtze Block (Zhou et al. 2002b) and bulk upper crust composition (Taylor and Mclennan 1985) have been added to Fig. 9 for reference. Therefore, we conclude that the parental magma of the Baimazhai intrusion probably had a composition similar to that of the Emeishan picrites. The modeling indicates that the extent of crustal contamination of the Baimazhai rocks varied from 4 to 35%, indicating a very strong upper crustal contamination.

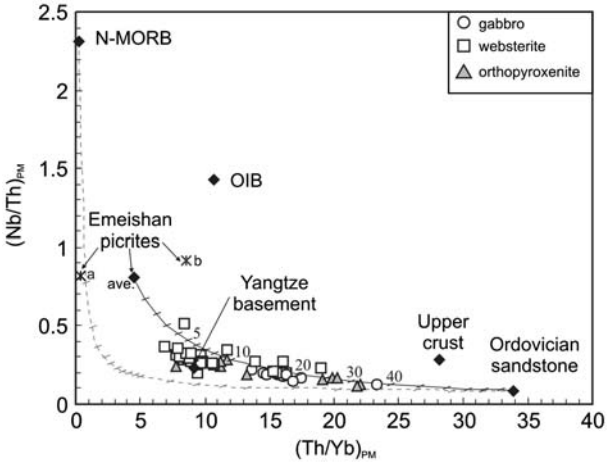

Fig. 9 $(Th/Yb)_{PM}$ versus $(Nb/Th)_{PM}$ diagram showing the high degree of crustal contamination of the Baimazhai rocks. Data source: N-MORB and OIB, Sun and McDonough (1989); Kangding complex, Zhou et al. (2002b); Emeishan picrites, Zhang et al. (2004) and our unpublished data; Upper crust, Taylor and Mclennan (1985); Country rocks (Ordovician sandstones), our data (Table 3)

Crystallization of Opx and segregation of sulfide by crustal contamination

The trigger for S-saturation and formation of the immiscible sulfide melts and the Opx crystals was undoubtedly crustal contamination. The assimilation of significant crustal material (especially silica) would have led to the fractionation of the magma and would force Opx, the main cumulus phase of both orthopyroxenites and websterites, onto the liquidus rather than olivine, consistent with that the inner core of the Baimazhai intrusion is composed of orthopyroxenites and that none of the Baimazhai samples plot close to the olivine control line in Fig. 3.

Crustal contamination of basaltic magmas would lower both the contents of FeO and temperature and thus lower the S capacity of the magma, resulting in sulfide over-saturation. In addition, contamination would probably have incorporated crustal S from the country rocks into the contaminated magmas (Keays 1995). Therefore, extensive crustal contamination was undoubtedly the trigger for S-saturation and formation of the immiscible sulfide melts in Baimazhai.

Cu/Zr ratios compare the concentrations of two highly incompatible elements, i.e., Cu, a highly chalcophile element, and Zr, non-chalcophile. These two elements are similarly incompatible during the early-stage fractional crystallization of sulfide-undersaturated mafic–ultramafic magmas. Typically chalcophile metal-undepleted continental flood basalts have Cu/Zr ratios around unity, whereas lavas depleted in chalcophile metals due to sulfide segregation have Cu/Zr ratios less than unity (Lightfoot and Keays 2005). Such a decrease in Cu/Zr ratios has been observed in the intrusive rocks at Voisey's Bay, Labrador, Canada and may have resulted from earlier sulfide segregation (Li and Naldrett 1999). The sulfide-poor gabbros and websterites of the Baimazhai intrusion with small Cu/Zr ratios (<1) (Fig. 7a) indicate that these rocks may have formed from magmas that had undergone sulfide segregation prior to emplacement, whereas the ''missing Cu'' resulted in much higher Cu/Zr ratios (3.3–2,240) in the orthopyroxenites.

During fractional crystallization of S-undersaturated magmas, the Pd/Cr ratio in residual magmas will increase because Cr enters the early-crystallized chromite whereas Pd is highly incompatible in chromite (Peck and Keays 1990). On the other hand, Pt/Y ratios in the residual magma will remain constant because Pt is mildly compatible in chromite (Peck and Keays 1990), whereas Y, like Zr, is highly incompatible in chromite. When immiscible sulfide segregation occurs in magmas, Pd/Cr and Pt/Y ratios in the residual magmas will dramatically decrease. In Baimazhai, the gabbros have the lowest Pd/Cr and Pt/Y ratios (Fig. 7b). The Pd/Cr and Pt/Y ratios of the orthopyroxenites and websterites have positive correlation and are dramatically decreasing (Fig. 7b). The gabbros with low Pd/Cr and Pt/Y ratios may represent the residual magma composition after the segregation of immiscible sulfide melts which were subsequently disseminated into the orthopyroxenites and websterites and resulted in their Pd/Cr and Pt/Y ratios higher than those for the gabbros. Therefore, the decrease of Pd/Cr and Pt/Y ratios from the orthopyroxenite, websterites, and gabbros, is consistent with sulfide removal segregation.

Emplacement of the Baimazhai intrusion by flow differentiation

The Baimazhai intrusion has a weighted average MgO content of 17.9% calculated on the basis of the average MgO contents of each orthopyroxenite, websterite and gabbro portions of the intrusion. About 70% of the Baimazhai intrusion is mineralized and massive sulfide ore body makes up 20 vol.% of the intrusion. The sulfides contents in the intrusion thus are much more than the magma can dissolve (c.f. Li and Riply 2005). Therefore, the low ratio of silicate melt volume to sulfide melt volume of the Baimazhai intrusion cannot be reached after emplacement. The excess magnesium components and sulfides in Baimazhai must have been derived from a much larger volume of magma than the intrusion itself. This may have been achieved by continuous flow of magma through a dynamic magma conduit or by repetitive replenishment of fresh magma into a large magma chamber (see Lesher and Keays 2002) or by flow differentiation in a dynamic magma conduit (Barker 1983).

In a magma conduit system, sulfide deposition is mainly controlled by fluid dynamics. The sulfide deposits are considered to have formed by large volumes of silicate magma passing through the conduit and leaving behind sulfide droplets together with early-crystallized silicate minerals, such as olivine (Naldrett and Lightfoot 1999). The sulfide ores usually occur at the bases of differentiated sills, like those in the Noril'sk region (Lightfoot and Keays 2005).

The uniform Pd/Pt and Cu/Pd ratios throughout the Baimazhai intrusion argue against multiple magma replenishment. The Pd/Pt ratio of the Baimazhai rocks average 1.9 (from 0.7 to 3.5), much lower than those (3–5) for Noril'sk (Lightfoot and Keays 2005). This is because the magmas which replenished the Noril'sk staging chamber had undergone extensive fractionation under S-undersaturated conditions before they entered the staging chamber. Under these conditions, the Pd/Pt ratio increases because the bulk partition coefficients are ~0.4 for Pd and ~1.0 for Pt (Lightfoot and Keays 2005). Both the Pd/Pt and Cu/Pd ratios are strongly affected by fractionation of magmas because of different partition coefficients for each of these elements (Lightfoot and Keays 2005). The fact that the ratios are similar in Baimazhai indicates that all the sulfides in Baimazhai were generated in a single sulfide segregation event in a staging magma chamber underlying the upper crust, where large amount of sulfide segregation and Opx crystallization occurred due to intensive crustal contamination. It is likely that both the immiscible sulfides and the Opx settled toward the base of the staging chamber. The magma chamber hence became stratified with sulfide- and phenocryst-free magma at its top and sulfide- and Opx phenocryst-laden magma at its base.

The Baimazhai intrusion probably formed in a convergent setting as the intrusion occurs along the boundary between the Indochina and Yangtze Blocks at the time when it formed during Permian time (Yan et al. 2006). The staging magma chamber was then evacuated from its top downward due to compressive forces. The concentrically zoned distribution of both sulfides and silicates in the Baimazhai intrusion can be explained by flow differentiation. The intrusion may have been a conduit for a flowing silicate melt laden with cumulus Opx crystals (~33 vol.% of the magma) and sulfide liquid (~20 vol.%). Due to higher velocity of magma in the center of the conduit and drag along its margins, both sulfides and Opx crystals were concentrated toward the center of the conduit because they both were denser than the carrier silicate melt. As a consequence, sulfide and Opx crystals are concentrated in center of the intrusion and decrease more or less systematically toward the margin of the intrusion.

The fractionated carrier magma may have intruded elsewhere or erupted to form lavas within the overlying volcanic succession. Lavas formed from such magmas should be recognized by high crustal contamination

signature and chalcophile metal depletion, similar to the Nadezhdinsky Formation of the Siberian Traps (Brugmann et al. 1993; Lightfoot and Keays 2005).

Conclusions

The ~260 Ma Baimazhai intrusion is part of the ELIP and is a concentric body with an inner core of orthopyroxenite rimmed by websterite and gabbro. The parental magmas of the intrusion were Si- and Mg-rich, S-undersaturated melts that became S-saturated before emplacement due to strong crustal contamination in a deep-seated staging magma chamber. Crustal contamination also prompted the crystallization of Opx which settled with the magmatic sulfides to the base of the staging chamber. The staging chamber was subsequently emptied from its top downward due to regional compressive forces. The magma forced out of the staging chamber flowed through the Baimazhai intrusion. Due to flow differentiation, sulfide melts and Opx crystals were more or less centrally disposed in the flowing magma to form the Baimazhai intrusion.

Acknowledgments This study was substantially supported by research grants from the Research Council of Hong Kong, China (HKU 7056/03P and HKU 7057/05P), an outstanding young researcher award from the National Nature Science Foundation of China (40129001) and a matching fund from the University of Hong Kong. The study was also partially supported by SEG 2005 Student Research Grants. The Baimazhai Mine Company is thanked for the assistance of field trip and the collection of drill core samples. We thank Mr L. Qi, Ms X. Fu and Ms Y. Liu for help with sample analyses. Thoughtful reviews by Dr C. Li and an anonymous referee helped to clarify the final version of this paper and are gratefully acknowledged.

References

Anders E, Grevesse N (1989) Abundances of the elements: meteoritic and solar. Geochim Cosmochim Acta 53:197–214

Arndt NT, Czamanske GK, Wooden JL, Fedorenko VA (1993) Mantle and crustal contributions to continental flood volcanism. Tectonophysics 223:39–52

Barker DS (1983) Igneous rocks. Prentice-Hall, Englewood Cliffs, pp 132–133

Barnes S-J, Naldrett AJ, Gorton MP (1985) The origin of the fractionation of platinum-group elements in terrestrial magmas. Chem Geol 53:303–323

Beswick AE (1982) Some geochemical aspects of alteration and genetic relations in komatiitic suites. In: Arndt NT, Nisbet EG (eds) Komatiities. George Allen& Unwin, London, pp 283–308

Brugmann GE, Naldrett AJ, Asif M, Lightfoot PC, Gorbachev NS, Fedorenko VA (1993) Siderophile and chalcophile metals as tracers of the evolution of the Siberian trap in the Noril'sk region, Russia. Geochim Cosmochim Acta 57:2001–2018

Chai G, Naldrett AJ (1992) Characteristics of Ni–Cu–PGE mineralisation and genesis of the Jinchuan deposit, Northwest China. Econ Geol 87:1475–1495

Chung SL, Jahn B-M (1995) Plume–lithosphere interaction in generation of the Emeishan flood basalts at the Permian–Triassic boundary. Geology 23:889–892

Guan T, Huang ZL, Xie LH, Xu C, Li WB (2003) Geochemistry of lamprophyres in Baimazhai nickel deposit, Yunnan Province: major and trace elements (in Chinese with English abstract). Acta Min Sin 23:278–288

Keays RR (1995) The role of komatiitic and picritic magmatism and S-saturation in the formation of the ore deposits. Lithos 34:1–18

Lesher CM, Keays RR (2002) Komatiite-associated Ni–Cu–(PGE) deposits. In: Cabri LJ (ed) The geology, geochemistry, mineralogy, mineral beneficiation of the platinum-group elements, vol. 54. Canadian Institute of Mining Metallurgy and Petroleum, Canada, pp 579–618

Lesher CM, Arndt NT, Groves DI (1984) Genesis of komatiite-associated nickel sulfide deposits at Kambalda, Western Australia: a distal volcanic model. In: Buchanan DL, Jone MJ (eds) Sulfide deposits in mafic and ultramafic rocks. Institute of Mining Metallurgy, London, pp 70–80

Li C, Naldrett AJ (1999) Geology and petrology of the Voisey's Bay intrusion: reaction of olivine with sulfide and silicate liquids. Lithos 47:1–31

Li C, Riply EM (2005) Empirical equations to predict the sulfur content of mafic magmas at sulfide saturation and applications to magmatic sulfide deposits. Miner Deposit 40:218–230

Lightfoot PC, Keays RR (2005) Siderophile and chalcophile metal variations in flood basalts from the Siberian Trap, Noril'sk Region: implications for the origin of the Ni–Cu–PGE sulfide ores. Econ Geol 100:439–462

Mahoney JJ (1988) Deccan traps. In: Macdougall JD (ed) Continental flood basalts. Kluwer Academic Publishers, Dordrecht, the Netherlands, pp 151–194

Naldrett AJ (2004) Magmatic sulfide deposit: geology, geochemistry and exploration. Springer, Berlin Heidelberg New York, pp 137–277

Naldrett AJ, Duke JM (1980) Platinum metals in magmatic sulfide ores. Science 208:1417–1428

Naldrett AJ, Lightfoot PC (1999) Ni–Cu–PGE deposits of the Noril'sk region, Siberia; their formation in conduits for flood basalt volcanism. In: Keays RR, Lesher CM, Lightfoot PC, Farrow CEG (eds) Dynamic processes in magmatic ore deposits and their application in mineral exploration, vol. 13. Geological Association of Canada, Short Course Notes, pp 195–249

Peck DC, Keays RR (1990) Insights into the behaviour of precious metals in primitive, S-undersaturated magmas: evidence from the Heazlewood River complex, Tasmania. Can Mineral 28:553–577

Qi L, Hu J, Gregoire DC (2000) Determination of trace elements in granites by inductively coupled plasma mass spectrometry. Talanta 51:507–513

Song XY, Zhou M-F, Wang YL, Zhang CJ, Cao ZM, Li Y (2001) Geochemical constrains on the mantle source of the Upper Permian Emeishan continental flood basalts, SW China. Int Geol Rev 43:213–225

Song XY, Zhou M-F, Cao Z, Sun M, Wang Y (2003) Ni–Cu–(PGE) magmatic sulfide deposits in the Yangliuping area, Permian Emeishan igneous province, SW China. Miner Deposita 38:831–843

Sun SS, McDonough WF (1989) Chemical and isotopic systematics of oceanic basalts: implications for mantle composition and processes. In: Saunders AD, Norry MJ (eds) Magmatism in the ocean basins, vol. 42. Special Publication, Geological Society of London, London pp 313–345

Sun SS, Nesbitt RW, McCulloch MT (1989) Geochemistry and petrogenesis of Archaean and early Proterozoic siliceous high-magnesian basalts. In: Crawford AJ (ed) Boninites. Unwin Hyman, London, pp 148–173

Taylor SR, Mclennan SM (1985) The continental crust: its composition and evolution, an examination of the geochemical record preserved in sedimentary rocks. Blackwell Science Publishing, Oxford UK, pp 312

Wang CY, Zhou M-F, Zhao DG (2005a) Mineral chemistry of chromite from the Permian Jinbaoshan Pt–Pd-sulphide-bearing ultramafic intrusion in SW China with petrogenetic implications. Lithos 83:47–66

Wang CY, Zhang Q, Qian Q, Zhou M-F (2005b) Geochemistry of the early Paleozoic Baiyin volcanic rocks (NW China): implications for the tectonic evolution of the North Qilian orogenic belt. J Geol 113:83–94

Xu YG, Chung SL, Jahn B-M, Wu GY (2001) Petrologic and geochemical constraints on the petrogenesis of Permian–Triassic Emeishan flood basalts in southwestern China. Lithos 58:145–168

Yan DP, Zhou M-F, Wang CY, Xia B (2006) Structural and geochronological constraints on the tectonic evolution of the Dulong–Song Chay tectonic dome in Yunnan Province, SW China. J Asian Earth Sci (in press)

YBGMR (Yunnan Bureau of Geology and Mineral Resources) (1990) Regional geology of Yunnan Province. Geological Memoirs, Ser. 1, No. 21. Geological Publishing House, Beijing, p. 554 (in Chinese)

Zhang HF, Sun M, Lu FX, Zhou XH, Zhou M-F, Liu YS, Zhang GH (2001) Moderately depleted lithospheric mantle underneath the Yangtze Block: evidence from a garnet lherzolite xenolith in the Dahongshan kimberlite. Geochem J 35:315–331

Zhang ZC, Wang FS, Hao YL, Mahoney JJ (2004) Geochemistry of the picrites and associated basalts from the Emeishan large igneous basalt province and constraints on their source region (in Chinese with English abstract). Acta Geol Sin 78:171–180

Zhou M-F, Malpas J, Sun M, Liu Y, Fu X (2001) A new method to correct Ni- and Cu-argide interference in the determination of the platinum-group elements, Ru, Rh, and Pd, by ICP-MS. Geochem J 35:413–420

Zhou M-F, Malpas J, Song XY, Kennedy AK, Robinson PT, Sun M, Lesher CM, Keays RR (2002a) A temporal link between the Emeishan large igneous province (SW China) and the end-Guadalupian mass extinction. Earth Planet Sci Lett 196:113–122

Zhou M-F, Yan DP, Kennedy AK, Li YQ, Ding J (2002b) SHRIMP U–Pb zircon geochronological and geochemical evidence for Neoproterozoic arc-magmatism along the western margin of the Yangtze Block, South China. Earth Planet Sci Lett 196:51–67

Zhou M-F, Robinson PT, Lesher CM, Keays RR, Zhang CJ, Malpas J (2005) Geochemistry, petrogenesis and metallogenesis of the Panzhihua gabbroic layered intrusion and associated Fe–Ti–V oxide deposits, Sichuan Province, SW China. J Petrol 46:2253–2280

Zhou M-F, Zhao JH, Qi L, Su W, Hu RZ (2006) Zircon U–Pb geochronology and elemental and Sr–Nd isotopic geochemistry of Permian mafic rocks in the Funing area, SW China. Contrib Mineral Petrol 151:1–19